INDOCHINA APPLIED SCIENCES

H. M. Kefas et al. / Indochin. Appl. Sci. 14(2) (2025) 255590

Research Article

Removal of Iron and Copper Ions from Water Using Cashew Nut Shell Adsorbent: Langmuir, Freundlich, Redlich-Peterson and Harkin-Jura Isotherms

Haruna Mavakumba Kefas, Yusufu Luka, Abdulhalim Musa Abubakar*, Augustine Odey Egbeji

Department of Chemical Engineering, Faculty of Engineering, Modibbo Adama University,Yola, Adamawa State, Nigeria

***Corresponding authors** *:* *abdulhalim@mau.edu.ng*
https://doi.org/10.55674/ias.v14i2.255590

Received: 02 February 2024; **Revised:** 07 July 2024; **Accepted:** 30 April 2025 ; **Available online:** 1 May 2025

Abstract

Elevated copper (Cu) and iron (Fe) levels can pose a threat to biodiversity. Removal of those metallic impurities was achieved in this study using cashew nut shell (CNS) adsorbent. Greater sorption of 87.40% Cu and 99.50% Fe occurred at 10 min contact time and 0.40 g CNS dosage. This study also targets the determination of the adsorption mechanism of the process, where it was discovered that it satisfied a favorable monolayer adsorption on homogeneous active sites at 1.1106 mg g $^{-1}$ Cu and 1.0995 mg g $^{-1}$ Fe uptakes (q_e), described by the Langmuir isotherm with R^2 value > 0.9990. The run essentially carried out using Lake Gerio water sample in Nigeria also satisfy the Redlich-Peterson model whose constant exponent, $\beta = 0.9773$ for Cu and 0.9985 for Fe ≅ 1, implied similar behavior with Langmuir isotherm assumption at specific temperature of 30°C. Effect of varying contact time and CNS dosage was also tested on % equilibrium sorption and q_e. Both Harkin-Jura and Freundlich equations poorly fit the empirical result with no match to adsorption evidence depicted after Fourier Transform Infrared (FTIR), Scanning Electron Microscopy (SEM) and Atomic Absorption Spectroscopy (AAS) analysis carried out. Removal of heavy metals such as Cu and Fe from lakes and rivers will contribute to benthic organisms and sediment quality, food chain integrity, fish and seafood safety, recreational use, human and environmental health. Thus, the potentials demonstrated by CNS in the removal of Cu and Fe in this study as well as other heavy metals already investigated, will ensure long-term ecosystem resilience.

Keywords*:* Cashew nut shell; Adsorption isotherm; Biosorption; Heavy metal; Adsorbent dosage.

1. Introduction

Langmuir, Freundlich, Redlich-Peterson, and Harkin-Jura are various isotherm models used to describe the adsorption of molecules onto a solid surface. These models help to understand and quantify the relationship between the amount of adsorbate (in this case, Cu & Fe) and its concentration in the solution at a constant temperature. Each isotherm model has its own strengths and weaknesses, and the choice of which to use depends on the specific characteristics of the adsorption system being studied, as well as their guided assumptions. In Langmuir [1 – 3], adsorption of one molecule does not affect the adsorption of neighboring molecules and adsorption occurs at specific homogeneous sites on the adsorbent surface, in which each adsorption site can accommodate only one molecule (monolayer adsorption). Redlich-Peterson retains the two assumptions in Langmuir, but incorporated an exponent, 'β', that allows for variation in adsorption energy with coverage. Meanwhile, Freundlich assumed that the adsorption occurs on a heterogeneous surface with different sites having different adsorption energies [4, 5]; in that case, a multilayer adsorption. Harkin-Jura introduces an exponential decay term to account for non-ideal behavior in the adsorption process and states further that the adsorption capacity is exponentially dependent on the function of concentration. Except in Redlich-Peterson isotherm, the 3 other models are valid only at a specific temperature. Adsorption studies to determine the choice and validity of adsorption isotherm models involves the use of adsorbents such as silica gel, hydrogels, molecular sieves, polymeric adsorbents, metal-organic frameworks, graphene-based materials, carbon nanotubes,

Montmorillonite clay, activated alumina, zeolites, activated carbon (AC) [6], pharmaceuticals [7] and biosorbents [8, 9]. Adsorbent choice should depend on their resistance to attrition, environmental compatibility, stability, ease of handling, porosity, high surface area, chemical inertness, availability, good kinetic, low cost, specific affinity and regenerability.

Cashew nut shell (CNS) is an agricultural biosorbent with high density [10] and a thickness of 3.20 mm [11] that embodied almost all these qualities, plus a significant amount of char obtainable via carbonization [12]. Reports shows that there is 80.4 mg kg^{-1} Cu and 7940 mg kg^{-1} of Fe in CNS ash [13] for CNS having 0.61% ash [14]. Sanger et al. (2011) reported that the shell covers 50% of the mass of the raw nut, the CNS liquid (CNSL) represents 25% and the remaining 25% consists of the kernel containing oil [16, 17]. Cashew nut tree (*Anacardium occidentale*) as a whole, is native of Peru and Brazil [18]. Statistics revealed that the previous production of CNS is around 310,000 tons [19], increasing to 800,000 to 835,000 to 856, 000 tons [20, 21]. Adsorbents are generally used to remove a wide range of adsorbates from gases, liquids, or solutions. Specific adsorbates removed are nitrogen oxides, phenols and organic pollutants [22], volatile organic compounds, dyes and pigments [23], water vapor, oxygen and nitrogen, radioactive substances, sulfur compounds, organic gases and vapors [14, 24], ammonia, proteins and enzymes, carbon dioxide, water hardness [25, 26] and heavy metals (e.g., Fe and Cu). Previous studies on the use of CNS adsorbent to remove diverse range of heavy metals adsorbates, is shown in Table 1.

Table 1 Isotherm studies of CNS bio-adsorbent to remove metallic adsorbates examined by different isotherm models.

Heavy Metal	**Model Employed**	**Adsorption Condition**	**Findings**	Study
Cu	Isotherm: Langmuir, Freundlich, Temkin & Dubinin–Radushkevich and Kinetic: Pseudo-First-order, Pseudo-Second-order, Intraparticle diffusion, Boyd, and shrinking core	pH, adsorbent dose, initial copper ions concentration, contact time & temperature	Spontaneous, feasible, and exothermic adsorption favored by Pseudo-Second-order and Freundlich models	[22]
Pb & Cd	Langmuir & Freundlich	Effect of contact time, initial heavy metal conc., initial pH & AC dosage	Both models are suitable with 99.9% & 28.90 mg g^{-1} Pb and 98.87% & 14.29 mg g^{-1} Cd removal % and capacity, respectively	[27]
Cu & Cr	Isotherm: Langmuir, Freundlich & Redlich–Peterson and Kinetic: Pseudo-First-order, Pseudo-Second-order & Intraparticle diffusion	0.10 g bio-adsorbent, pH 5, room temp. & 10 –100 mg L^{-1} metal conc.	Langmuir & Pseudo-Second Order are best with 91% & 49.80 mg g^{-1} Cu and 96% & 41.77 mg g^{-1} Cr % removal and max. adsorption capacity, respectively	[28]
Ni	Isotherm: Langmuir, Freundlich, Temkin & Dubinin–Radushkevich and Kinetic: Pseudo-First-order, Pseudo-Second-order & Elovich	Sorption as function of parameters such as solution pH, CNS dose, contact time, initial Ni conc. & temp.	Both Langmuir & Freundlich are suitable with 18.868 adsorption capacity	[2]
Fe	Isotherm: Langmuir & Freundlich and Kinetic: Pseudo-First-order & Pseudo-Second-order	Effect of particle size (90 μm), adsorbent dosage (0.20 g), initial iron concentration, contact time (60 min), pH (5) and temperature	Langmuir & Pseudo-Second Order is the best with 73.05% removal and 200 mg g^{-1} max. adsorption capacity	[29]
Cr	Langmuir & Freundlich	12.50 mg AC, 2-5 pH, 250 μm particle size, 24 h contact time and 10, 40 & 100 mg L^{-1} Cr conc.	Max. adsorption capacity from Langmuir = 320 –340 mg g^{-1} (best model)	[30]

Cr	Langmuir & Freundlich	Optimal experimental parameters: pH (3.50), contact time (60 min), dosage of adsorbent (1.20 g) & initial conc. Of Cr solutions (100 mg L^{-1})	Best fit is Langmuir with 13.93 mg g^{-1} max. adsorption capacity	[31]
Pb	Isotherm: Langmuir, Freundlich, Temkin & Dubinin–Radushkevich and Kinetic: Pseudo-First-order, Pseudo-Second-order & Elovich	Varying the solution pH, initial Pb conc. (100 – 500 mg L^{-1}), contact time & temperature (30 – 60 °C) at 1g/L dosage	Freundlich & Pseudo-Second order are the best fitting with 408.60–480.50 mg g^{-1} max. Pb uptake	[32]
Cd	Isotherm: 2-parameter (Langmuir, Freundlich, Temkin & Dubinin-Radushkevich) and 3-parameter (Redlich-Peterson, Koble-Corrigan, Toth & Sips) and Kinetic: Pseudo-First-order, Pseudo-Second-order, Elovich & Intraparticle diffusion	30 – 60°C temp., 2 – 8 pH, 10 – 50 mg L^{-1} Cd initial conc. & 5 – 60 min	Monolayer Cd uptake is 22.11 mg/g, but Freundlich is the best, as well as Pseudo-Second order	[4]
Pb	Isotherm: Langmuir, Freundlich, Temkin & Dubinin–Radushkevich and Kinetic: Pseudo-First-order, Pseudo-Second-order, Elovich & Intraparticle diffusion	Effect of varying initial Pb conc. From 10 – 50 mg L^{-1}	Best fittings are Langmuir and Pseudo-First order. Predicted max. Pb uptake = 8.734 mg g^{-1}	[33]
Cd, Pb, Fe, Cu & Cr	Freundlich Isotherm	24h contact time and 1, 2, 3, 4 & 5 incremental weight of CNS- powdered AC	Pb sorption is higher. But % removal is 100, 98, 96, 94 & 87%, respectively	[34]
Cu	Isotherm: Langmuir & Freundlich and Kinetic: Pseudo-First-order, Pseudo-Second-order, Elovich & Intraparticle diffusion	Temp., initial Cu conc., 30 min contact time, pH 5 & CNS conc.	Sorption is feasible, spontaneous & exothermic and described by Pseudo-Second order	[35]
Zn	Isotherm: Langmuir, Freundlich, Temkin & Dubinin–Radushkevich and Kinetic: Pseudo-First-order, Pseudo-Second-order, Intraparticle diffusion & Boyd	At 30 °C, 30 min contact, pH 5, 3 g L^{-1} dose & 10 – 50 mg L^{-1} initial ion conc.	Good fits are Langmuir & Pseudo-Second order	[5]
Cd	Isotherm: Langmuir, Freundlich & Temkin and Kinetic: Pseudo-First-order & Pseudo-Second-order	Blend of coconut shell and CNS AC (1:1): 10 mg L^{-1} of Cd, 0.04g carbon dosage, 45 min time & pH 4	Pseudo-Second order and Langmuir model best describe the sorption process	[1]
Cd, Pb & Cr	Isotherm: Langmuir, Freundlich & Dubinin–Radushkevich and Kinetic: Pseudo-First-order, Pseudo-Second-order, Elovich & Intraparticle diffusion	12 g L^{-1} adsorbent mass (600 mg), pH = 5 & 60 min equilibrium time	All isotherms are suitable but only Pseudo-Second order kinetic was best	[36]

Cd, Pb & Cr	Isotherm: Langmuir, Freundlich & Dubinin–Radushkevich and Kinetic: Pseudo-First-order, Pseudo-Second-order, Elovich & Intraparticle diffusion	pH = 5, CNS mass/water volume = 0.40 g L^{-1} & 40 min contact time	Good fit by Langmuir, Freundlich & Pseudo-Second order	[20]
Cd & Pb	Isotherm: Langmuir & Freundlich and Kinetic: Pseudo-First-order & Pseudo-Second-order	Effect of contact time, adsorbent mass (12 g L^{-1}), initial ion conc. & pH (5)	94 – 99% Pb & 86 – 94% Cd removal were Freundlich describe Pb sorption better; but both ions follow Pseudo-Second order	[37]
Pb	Isotherm: Langmuir, Freundlich & Dubinin–Radushkevich and Kinetic: Pseudo-First-order, Pseudo-Second-order, Intraparticle diffusion & Boyd	20 mg L^{-1} Pb^{2+} initial conc., pH of 5, 30 min, 30 °C & 0.30 g CNS	Best correlation is Freundlich & Pseudo-Second order with 88.49% adsorption efficiency & 17.82 mg g^{-1} capacity	[38]
Cu & Fe	Langmuir, Freundlich, Redlich–Peterson & Harkin-Jura	4 L distil water, 0.11 mol L^{-1} NaOH, 200 g CNS, 0.63 mg L^{-1} Cu conc. 0.17 mg L^{-1} Fe conc., 0.40 – 1.60 g CNS dose, 30 °C, 10 – 60 min time & pH = 8.05	Best fit is Langmuir & Redlich-Peterson with actual max. uptake = 1.11 mg g^{-1} and predicted = 1.1106 mg g^{-1} Cu & 1.0995 mg g^{-1} Fe (at 0.40 g dosage)	This Study

Presence of one of all of Fe and Cu in several Nigerian waters, namely: Mada River [39, 40], River Ngadda [41], Alau Dam or reservoir [42, 43], Lake Gerio [44], Usuma Dam [45, 46], Jakara River [47, 48], River Challawa [49], Kusalla Dam [50] and Shinko drainage systems [51], to mention a few, often necessitates the study of their removal strategy. Their presence in water can contribute to corrosion of pipes, water distribution systems, leaks, pipe failures, damage of infrastructure and damage to plumbing systems. Guillaume et al. (2019) and Hunaidah et al. (2019) examined the purification of water using CNS AC without studying their isotherms and kinetics. Limitation in Yahya et al. (2020)'s work is also the non-study of kinetics of Cr and Mn sorption using CNS. For large scale remediation activity, kinetics and isotherms model parameters will enable the selection of optimal adsorption conditions. Therefore, the objectives of this study are to fit Fe and Cu sorption experimental data to four isotherm models to determine the parameters that best describe the adsorption process under certain conditions. To this end, in the literature (Table 1), Pb, Cu, Cr, Fe, Ni, Zn, Mn and Cd removal from aqueous water solution had been carried out using CNS and their adsorption mechanism studied using selected adsorption isotherms. Cu and Fe were chosen for removal in this study due to their widespread presence in water in Nigeria, potential toxicity, effects on water quality, and the need to comply with regulatory standards. CNS use as adsorbent is advantageous, given that it is inexpensive and sustainable for large-scale use, in addition to having a large surface area and containing some lignocellulosic materials. Its frequent use is not constrained by its low mechanical strength, variability in composition, limited reusability, slow adsorption rate, need for pre-treatment and toxicity. As observed, not all isotherm studies were conducted for a particular heavy metal. By applying Langmuir, Freundlich, Redlich-Peterson, and Harkin-Jura models on experimented Cu^{2+} and Fe^{2+} laboratory data, this study brings into cognizance, the performance of unexploited isotherms (especially the Redlich-Peterson and Harkin-Jura models) for water purification using CNS. Coupled with the abundance of cashew nut in the country: i.e., 636,000 tons/y [13] and 100,000 metric tons produced in 2019 alone [11], CNS may champion the removal of the majority of heavy metals present in water, as evidenced in success reports/findings of Table 1, as one of the chief and sustainable adsorbent. In those studies, and as carried out herein, Scanning Electron Microscopy (SEM), Energy-Dispersive X-Ray (EDX) Spectroscopy, Fourier Transform Infrared (FTIR) Spectroscopy and Atomic Absorption Spectroscopy (AAS) analysis will help validate the occurrence of biosorption of the heavy metals.

Thus, the keywords in this study were carefully selected so that it aligns with the environmental engineering aspect of chemical engineering that deals with pollution control, waste treatment and environmental protection. Due to growing interest in these sub-fields, the keywords search in science direct between 2019-2023 alone, returns a somewhat ever-increasing

appearance in titles of article types that comprised of review, research articles, encyclopedia and book chapters, as shown in Fig. 1.

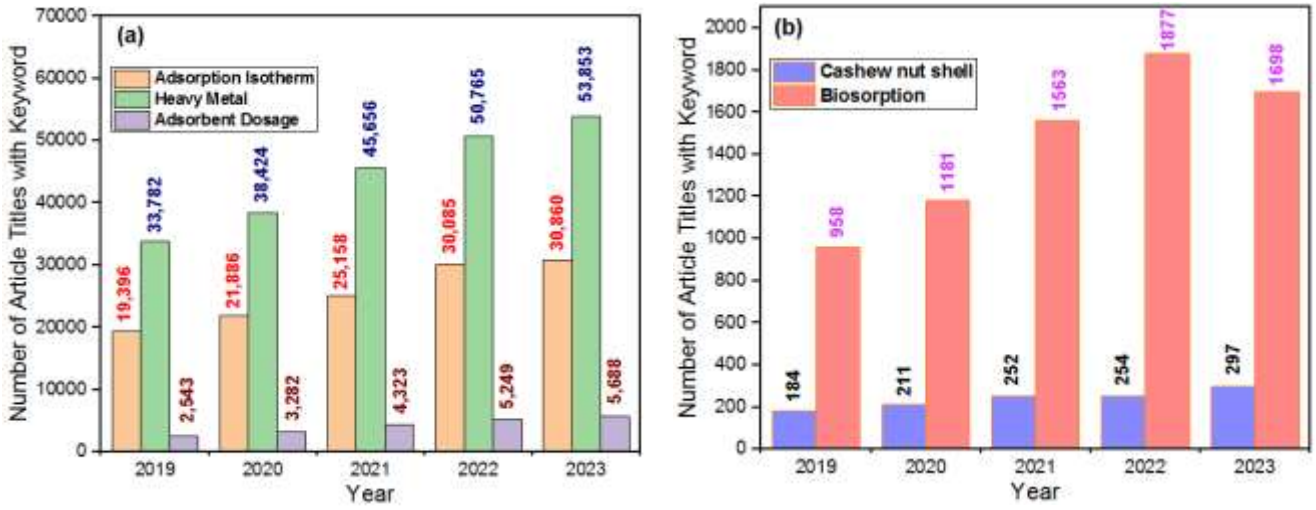

Fig. 1 Number of published works with this study's keywords.

2. Materials and Methods

2.1 Reagents and Apparatus

In this study, 4 L of distilled water, 0.11 mol L^{-1} of sodium hydroxide (NaOH) and 200 g of cashew nut shell (CNS) were used for washing, oil removal from the CNS sample and the adsorption of Fe^{2+} and Cu^{2+} ions, respectively. SEM, EDX, FTIR and AAS machines were employed in the study. All experiments were run using reagents, materials and equipment domicile at Modibbo Adama University Central Laboratory, and other locations in Nigeria.

2.2 CNS Biosorbent Preparation

Nut shells of the cashew plant were collected from cashew tree. Seeds collected were initially washed to remove impurities attached [55], sun-dried and grinded to < 2 mm powder. Grounded solid was extracted with the use of hexane to remove CNS liquid and the remaining shells were dried at 105 °C for 24 h. Portions of the shell were treated with 1m each of aqueous solutions of NaOH at 30 °C for 24 h. Subsequently, it was washed with distilled water severally until the pH of the water equals 6.90. The chemically treated adsorbent was later dried at 105 °C for 1 h and kept in a desiccator before use. There is however, an observed weight loss due to damaged CNS structure, dissolution of some compositions and operational washing, filtering and drying stages.

2.3 Characterization

Using Perkin Elemer Spectrum V10.4.3 FTIR machine, functional group taking part in the adsorption of the metal ions were determined and analyzed. DW-AA4530F AAS spectrophotometer used, gives the atomic and weight concentrations of entire elements present in the CNS before and after adsorption. During AAS analysis, mixture of the biosorbent and wastewater was centrifuged and filtered to obtain a clear supernatant (aqueous sample), which was then analyzed for each metal ion concentration.

2.4 Removal Efficiency and Metal Uptake

Equations (1) and (2) [56] were used to determine the equilibrium adsorption capacity or metal uptake, q_e (mg g^{-1}) and the percent removal (%) or removal efficiency (RE), respectively.

$$q_e = \frac{V(C_i - C_e)}{M} \quad (1)$$

$$RE = \frac{C_i - C_e}{C_i} \times 100 \quad (2)$$

Initially, varying biosorbent dosage (M) of 0.40, 0.80, 1.20 and 1.60 g weighed using ALE-223 electric balance, were added to four containers containing equal volume of Lake Gerio water sample to form a solution of volume, V. Prior to the mixing, pH of the surface water was measured using a pH meter, in addition to the initial Cu and Fe ions present (C_i) using AAS equipment. Final concentrations of metallic ions presence after adsorption (C_e) for each container and at varying contact time of 10, 20, 40 and 60 mins, were determined at 30 °C.

2.5 Isotherm Parameter Determination

Linearized form of the Langmuir, Freundlich, Redlich-Peterson and Harkin-Jura isotherm models given in Eq. (3) – (6) respectively [57], were used to determine the isotherm parameters based on the metallic ion data that gives the highest RE for a particular CNS dose.

$$\frac{C_e}{q_e} = \frac{C_e}{q_{max}} + \frac{1}{q_{max}\, k_L} \quad (3)$$

$$\log q_e = \frac{1}{n} \log C_e + \log K_f \quad (4)$$

$$\ln\left(\frac{C_e}{q_e}\right) = \beta \ln C_e - \ln A_{RP} \quad (5)$$

$$\frac{1}{{q_e}^2} = \frac{B}{A} - \left(\frac{1}{A}\right) \log C_e \quad (6)$$

Where, q_{max} = maximum monolayer adsorption capacity of CNS adsorbent (mg g^{-1}), k_L = Langmuir adsorption constant (L mg) $^{-1}$, K_f = Freundlich constant incorporating the factors affecting q_e, n = Freundlich constant incorporating the factors affecting adsorption intensity, A_{RP} = Redlich-Peterson model isotherm constant (L g^{-1}), β = Redlich-Peterson model exponent ($0 \leq \beta \leq 1$) and A & B = Harkin-Jura constants. An additional Langmuir parameter called 'dimensionless separation factor', R_L was calculated to explain the feasibility of the sorption process using Eq. (7).

$$R_L = \frac{1}{1 + k_L C_i} \quad (7)$$

Relevant linear plots were conducted, where these unknown parameters were calculated or extracted from the slopes and intercepts observed.

Prepare titanium (IV) isopropoxide volume 10 ml, dissolve in ethanol (C2H5OH, Merck, 99.50%) volume 100 ml, and dissolve silver nitrate ($AgNO_3$, VWR Prolabo, United Kingdom) volume 1, 2, 4, 8, 16 mol percent in Ethanol volume 50 ml. Adjust the pH with Sodium hydroxide at a concentration of 2 mol. It regulates the pH at about 6 to achieve a precipitation reaction. Dry the solution at 100 °C for 12 h. Calcined the synthetic powder at 500 °C for 1 h.

2.2 Characterizations

The Surface morphology and the size of TiO_2 nanoparticles were visualized using TEM (JEM-2010, JEOL). SEM with EDX spectrum was recorded with the help of Quanta FEG-250 to determine its homogeneity and its elemental distribution of elements in the investigated compound X-Ray Diffraction pattern of investigated TiO_2 nanoparticles was recorded by using (Phillips X'pert MPD, Cu-K). Structure of doping was determined by X-ray Photoelectron Spectroscopy (XPS, AXIS Ultra DLD, Kratos analytical Ltd.).

3. Results and Discussions

3.1 FTIR of CNS Before and After Sorption

In the region of 800 and 4000 cm^{-1} wave number, **%** transmittance of existing functional groups facilitating metallic adherence to the biomass sorbent was carried out**.** FTIR spectrum of CNS obtained prior to the adsorption process **(**Fig**.** 2**)** provides a detailed glimpse into its molecular composition and also the peaks of various functional groups on the samples**.** FTIR spectrum of CNS is pivotal not only for characterizing its nutritional composition but also for potential applications in the food industry and health research**.**

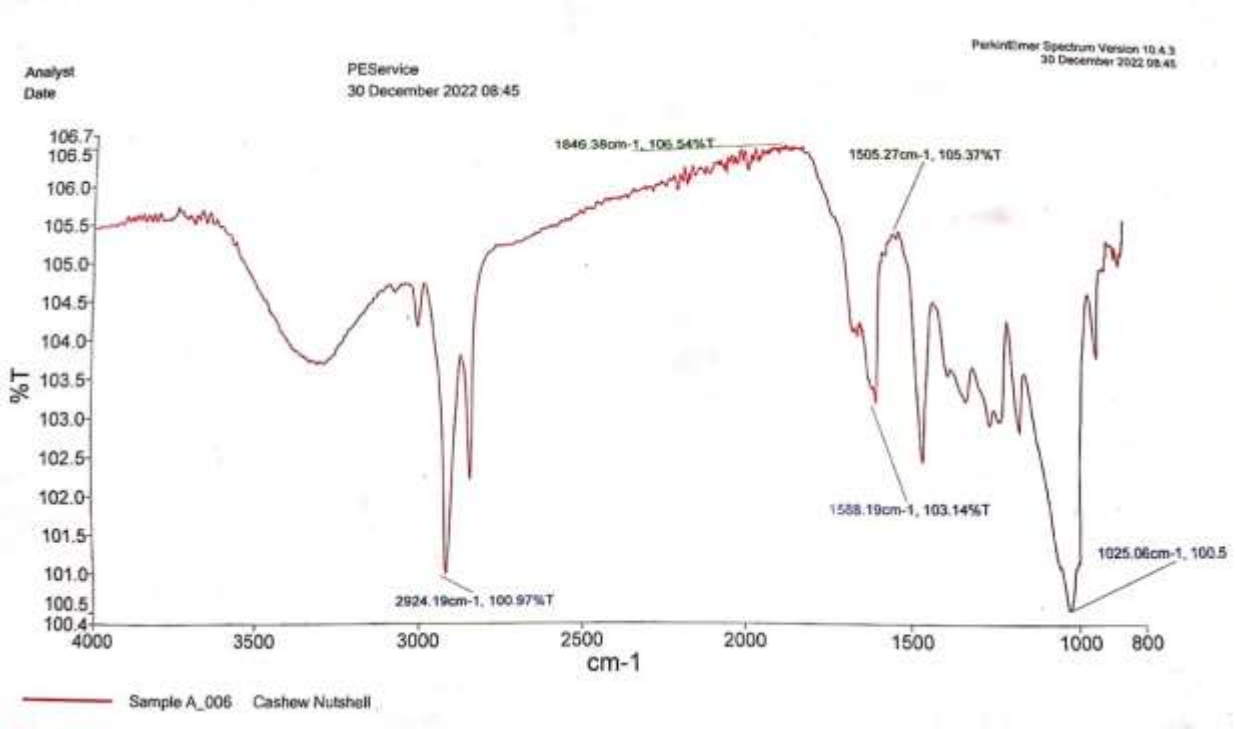

Fig. 2 FTIR of CNS before metal ions adsorption unto surface**.**

Dominant peak at 2924**.**19 cm^{-1} in Fig**.** 2, is indicative of aliphatic compounds, suggesting a substantial presence of lipids and carbohydrates in the sample, as described in Luka et al**. (**2023**).** These are essential components commonly found in nuts and contribute to their nutritional profile**.** Intriguingly, the peak at 1846**.**38 cm^{-1} stands out as an anomaly, and its origin warrants further investigation**.** It could be associated with a unique functional group specific to CNS or may be influenced by experimental factors**.** In the context of natural products like nuts, variations in growing conditions and geographical origin can lead to distinct molecular profiles**.** Moving to the mid**-**range of the spectrum, the peak at 1588**.**19 cm^{-1} suggests the presence of C=C stretching vibrations, typical of aromatic compounds **[**33**].** This finding aligns with the expected presence of phenolic compounds in the CNS, known for their antioxidant properties, as reported also by Tangjuank et al**. (**2009a**).** Additionally, the peak at 1505**.**27 cm^{-1} indicates the possibility of amines or proteins **[**3**]**, contributing to the overall nutritional content of the nut**.** The lower intensity peak at 1025**.**06 cm^{-1} corresponds to C**-**O stretching vibrations, characteristic of carbohydrates,

aligning with the known carbohydrate content in nuts, which provides energy and dietary fiber. Same FTIR analysis result is reported post-adsorption in Fig. 3.

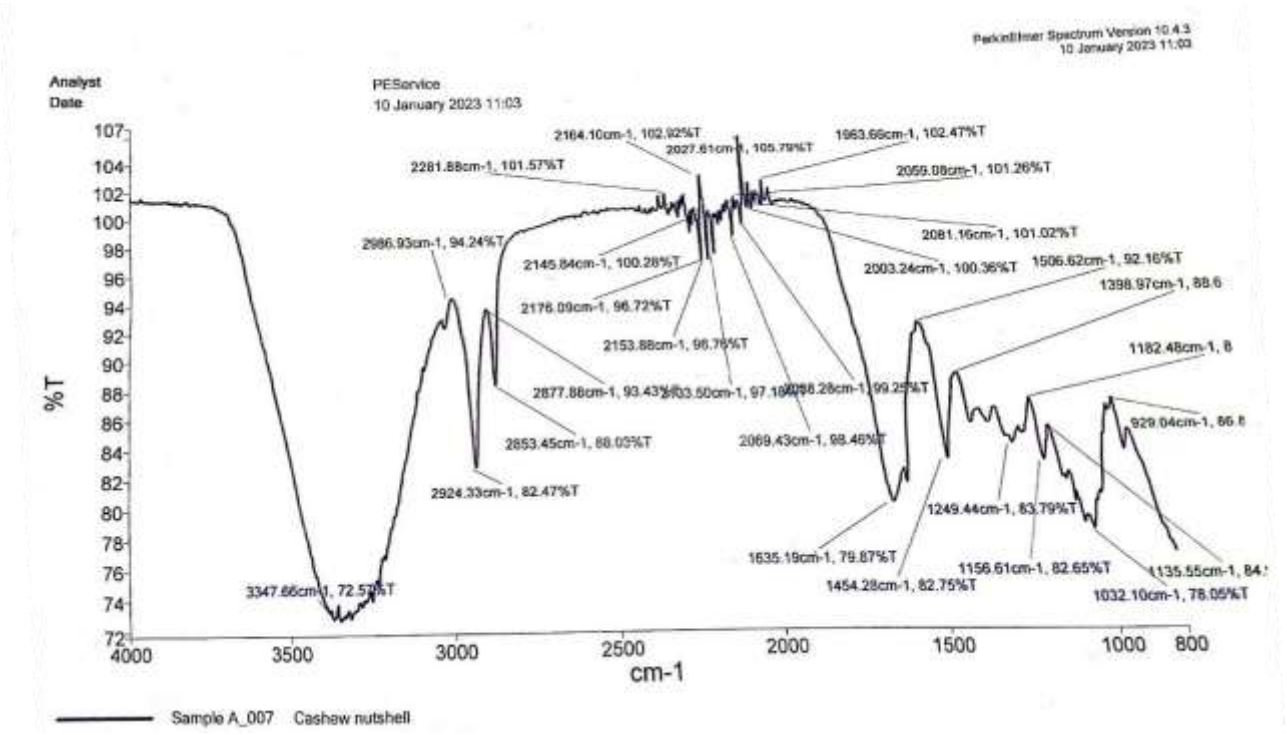

Fig. 3 FTIR of CNS after metal ions adsorption unto surface.

At 3347.66 cm^{-1}, a decrease in absorbance to 72.57 suggests effective water adsorption [4, 33], aligning with the anticipated removal of water impurities from the Lake Gerio samples. The peak at 2983.96 cm^{-1}, associated with C-H stretching vibrations in aliphatic compounds, displays an increase in absorbance, representative of additional adsorption of organic impurities. Concurrently, the peaks at 2924.33 and 2853.45 cm^{-1}, attributed to C-H stretching vibrations, demonstrate alterations in the composition of aliphatic compounds, possibly reflecting changes due to the adsorption process. Noteworthy peak at 2281.88 cm^{-1} is distinctive and suggests a significant change in the molecular composition of CNS post-adsorption, possibly reflecting the unique impurities present in Lake Gerio water. Peaks associated with C≡C stretching vibrations (2178.09 cm^{-1}) and C=O stretching vibrations (2164.10 cm^{-1}) exhibit increased absorbances, signifying potential adsorption of unsaturated and carbonyl-containing compounds [31] from the lake water. The peaks at 2145.84, 2133.50 and 2069.43 cm^{-1} associated with C-H bending vibrations, persist, suggesting the continued presence of aliphatic compounds in the adsorbed state. A noteworthy change is observed in the region around 2027.61 cm^{-1}, associated with N-H bending vibrations [30], suggesting potential adsorption of nitrogen-containing impurities. Peaks related to C=C stretching vibrations in aromatic compounds (1635.19 cm^{-1} and 2069.43 cm^{-1}) exhibit altered absorbances, indicating variations in the concentration of aromatic compounds post-adsorption, as explained in Haneef & Nair (2017) and Coelho et al. (2018). The peak at 1032.10 cm^{-1}, linked to C-O stretching vibrations, displays a decrease in absorbance, signifying changes in the concentration of carbohydrates or other oxygen-containing compounds in the adsorbed state. Additionally, the peak at 1156.61 cm^{-1}, associated with C-N stretching vibrations, demonstrates changes in the concentration of nitrogen-containing compounds. Finally, the band at around 1617 cm^{-1} can be attributed to aliphatic and/or unsaturated aromatic compounds present. Again, slight variation in the intensity and nature of the FTIR peaks of the samples before and after the adsorption shows that there was sorption of Cu and Fe ions. Smith et al. (2021) and de Oliveira et al. (2021) reported that the existence of quite a few functional groups such as -OH (hydroxyl), -CH (carboxylate) and -C = O (carbonyl), indicates the occurrence of adsorption of metals, as they act as active sites, contributing to a good performance of the CNS material.

3.2 EDX Spectra of CNS

EDX is a technique used to analyze the elemental composition of a sample by detecting characteristic X-rays emitted when the sample is irradiated with high-energy X-rays. Elements listed within the table of Fig. 4 include carbon (C), nitrogen (N), potassium (K), silver (Ag), magnesium (Mg), sodium (Na), aluminium (Al), silicon (Si), calcium (Ca), sulfur (S), phosphorus (P), iron (Fe), and chlorine (Cl), along with their corresponding atomic and weight concentrations were detected in the CNS before and after its use as adsorbent.

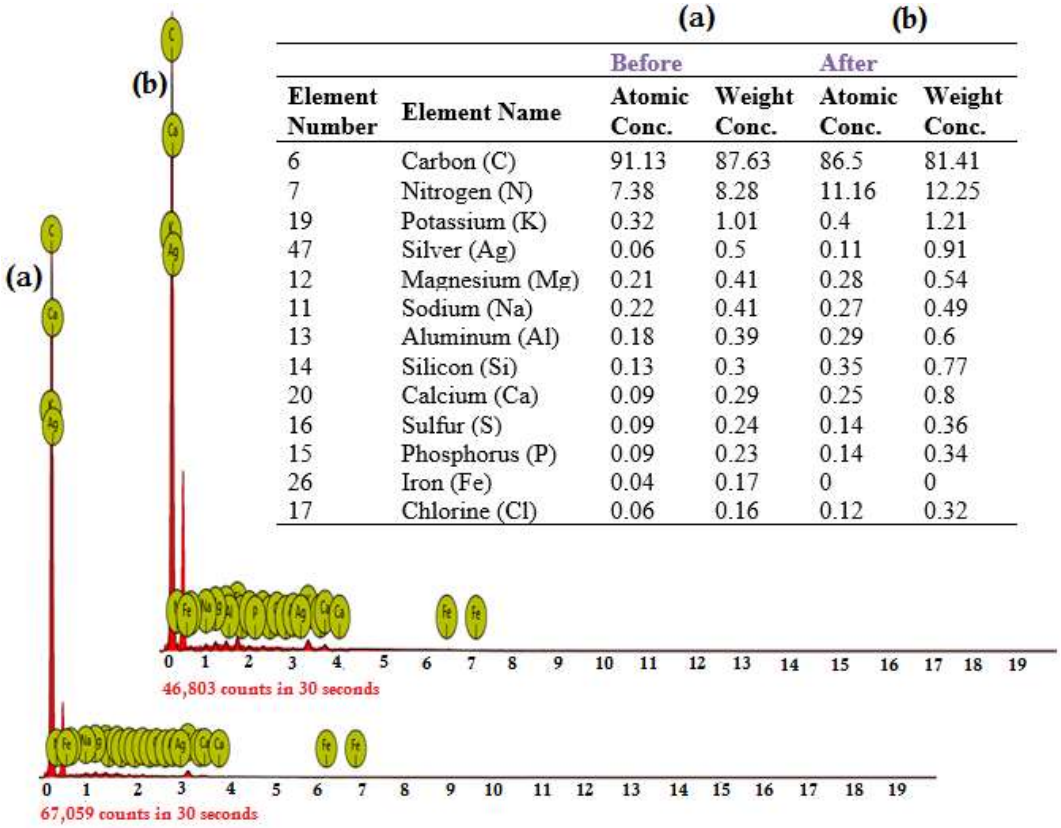

		(a) Before		(b) After	
Element Number	**Element Name**	**Atomic Conc.**	**Weight Conc.**	**Atomic Conc.**	**Weight Conc.**
6	Carbon (C)	91.13	87.63	86.5	81.41
7	Nitrogen (N)	7.38	8.28	11.16	12.25
19	Potassium (K)	0.32	1.01	0.4	1.21
47	Silver (Ag)	0.06	0.5	0.11	0.91
12	Magnesium (Mg)	0.21	0.41	0.28	0.54
11	Sodium (Na)	0.22	0.41	0.27	0.49
13	Aluminum (Al)	0.18	0.39	0.29	0.6
14	Silicon (Si)	0.13	0.3	0.35	0.77
20	Calcium (Ca)	0.09	0.29	0.25	0.8
16	Sulfur (S)	0.09	0.24	0.14	0.36
15	Phosphorus (P)	0.09	0.23	0.14	0.34
26	Iron (Fe)	0.04	0.17	0	0
17	Chlorine (Cl)	0.06	0.16	0.12	0.32

Fig. 4 EDX Spectra of CNS (a) Before and (b) After adsorption.

Presence of elements like C, N, K, Mg, and others can be correlated with specific cellular or organic structures within the CNS. C is a fundamental component of organic matter, while elements like K and Mg are essential for plant growth and metabolism. Comparative analysis of EDX data before and after adsorption unveils significant shifts in the elemental composition of the CNS sample. Prior to adsorption (Fig. 4(a)), the predominant elements were C and N, with distinct concentrations of K, Ag, and various trace elements. Post-adsorption (Fig. 4b), noteworthy changes include a decrease in C concentration and a substantial increase in N, indicating alterations in the nut's chemical composition. K and Ag also exhibit noticeable variations. Elements such as Mg, Na, Al, Si, Ca, S, P, Fe, and Cl display diverse changes, including decreases in concentration or complete absence. These alterations suggest the impact of the adsorption process on the surface composition of the CNS.

3.3 SEM Images of Adsorbent

SEM provides high-resolution images, allowing for the observation of surface details. In the case of CNS, SEM revealed the microstructure of the nut's surface showing a rather smooth-like texture with pores and cracks, as revealed by Fig. 5. High magnification of up to 1000× showed this arrangement of cellular structures. SEM images after adsorption (Fig. 6) revealed shifts in surface morphology. Changes in texture, pore structure, and the presence of adsorbate particles were apparent.

Elemental distribution on the surface exhibited area with elevated concentrations of adsorbed elements, particularly N and Ag, providing insights into the sites of adsorption**.** Moreover, the SEM image after adsorption also indicate the introduction of new elements or contaminants, visible as foreign particles or deposits**.**

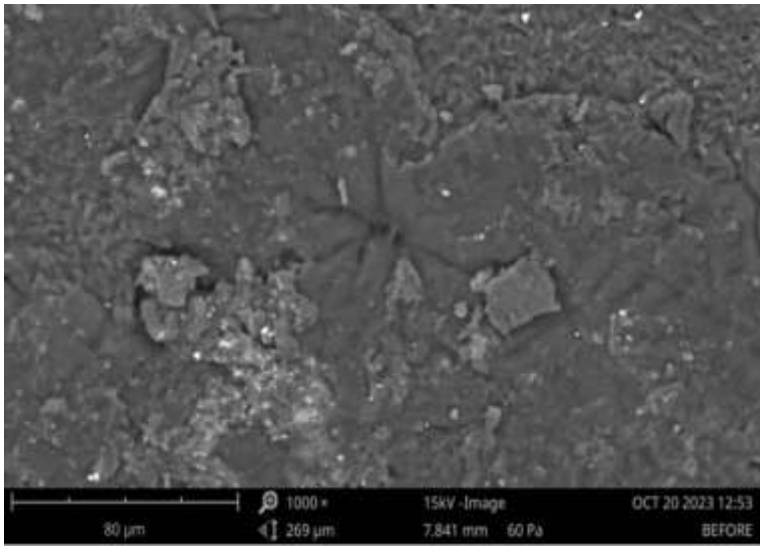

Fig. 5 CNS SEM at 1000 × magnification before metal ions adsorption

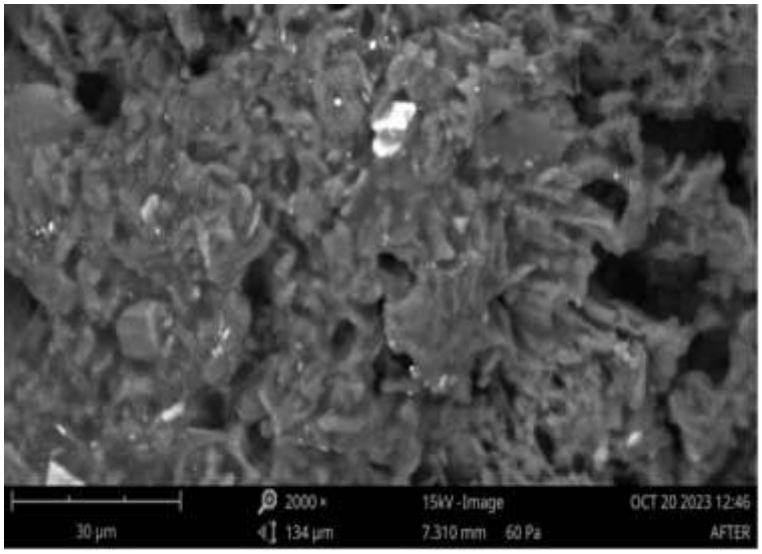

Fig. 6 CNS SEM at 1000 × magnification after metal ions adsorption**.**

After adsorption, an irregular morphology was observed in Fig**.** 6 due to pretreatment with an alkaline agent, instigating fiber swelling and resulting in its rupture**.** This process favors the appearance of pores**.** However, in Fig**.** 5, it is not possible to observe the superficial porous channels as was observed on the CNS after adsorption in Fig**.** 6**.** It may be concluded that the surfaces **(**porousness and sufficient surface area**)** of the biosorbent have a spongy, irregular and heterogeneous structure**.** According to de Oliveira et al**. (**2021**)** and Haneef & Nair **(**2017**)**, those characteristics favor the adsorption of metals, including Cu and Fe in aqueous solution**.**

3.4 Effect of Contact Time on Adsorption Capacity

Metal uptake of Lake Gerio surface water with 8.05 pH at different adsorbent dosage and contact time is tabulated in Table 2. As observed, q_e obtained for all CNS dose employed are within 1.07 – 1.11 mg g^{-1} Cu^{2+} and 1.09 – 1.11 mg g^{-1} Fe^{2+} uptake.

Table 2 Calculated metal uptake at Various CNS adsorbent weight.

Metal	**Contact Time**	**Adsorbent Dosage**			
		0.40 g	0.80 g	1.20 g	1.60 g
	t (min)	q_e **(mg** g^{-1}**)**	q_e **(mg** g^{-1}**)**	q_e **(mg** g^{-1}**)**	q_e **(mg** g^{-1}**)**
Cu^{2+}	0	0	0	0	0
	10	1.07	1.07	1.09	1.10
	20	1.08	1.09	1.10	1.10
	40	1.09	1.09	1.10	1.10
	60	1.10	1.11	1.11	1.11
Fe^{2+}	0	0	0	0	0
	10	1.09	1	1.10	1.10
	20	1.09	1.10	1.11	1.10
	40	1.10	1.10	1.11	1.10
	60	1.10	1.11	1.11	1.10

It shows that there is almost equal rate of metallic adherence to the CNS adsorbent at the specified contact time of 10 – 60 min. In this kind of situation, the lowest dosage of 0.40 g may be utilized for the sorption of Cu and Fe from Lake Gerio in order to conserve the generated adsorbent. Table 2 also recorded many constant q_e – for example, at 10 min when the dose is raised between 0.40 – 0.80 g (Cu2+ sorption) and 1.20 – 1.60 g (Fe2+ sorption) and at 20 – 60 min. Situations like that are attributed to saturation of active sites on the CNS surface or inadequate contact between the adsorbent and the adsorbate. Presumably, optimal dosage beyond which additional CNS adsorbent does not significantly enhance the q_e is attained. In this study, $q_e \cong$ 1.10 mg g^{-1} appears to be the equilibrium adsorption capacity, attained with the addition of 1.20 and 1.60 g CNS, as depicted in Fig. 7.

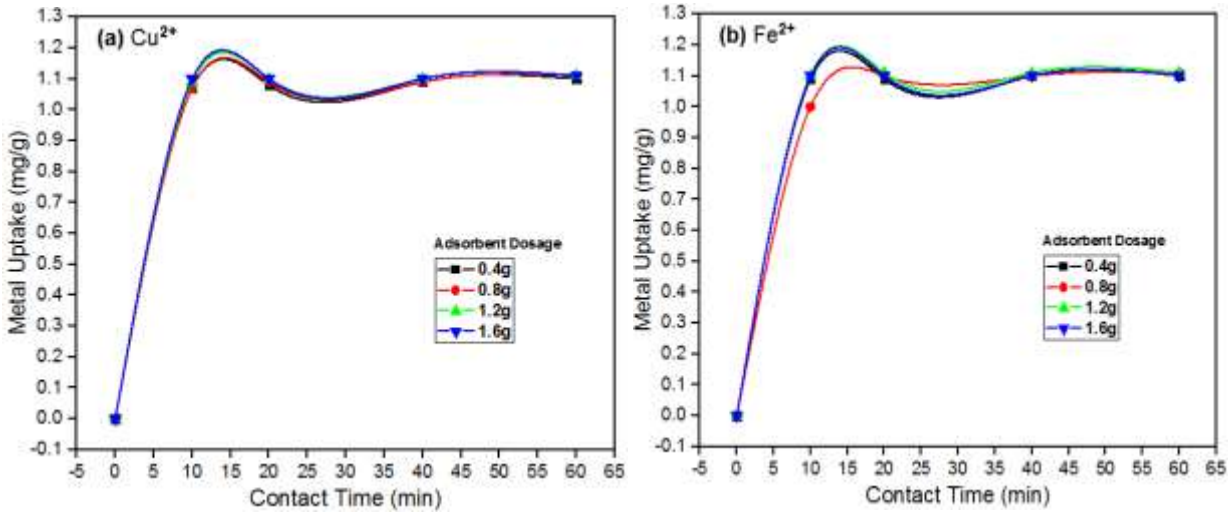

Fig. 7 Influence of Time and Dosage on (a) Cu^{2+} and (b) Fe^{2+} Uptake.

This peak value for q_e was sharply reached by Fe^{2+} sorption between 0.40 – 0.80 g dose but slowly between 0.40 – 1.20 g CNS dosage by Cu^{2+}. Though the speed or time before it is attained is very low, the CNS adsorbent demonstrates faster adsorption of Fe^{2+} than Cu^{2+} from the water sample. However, it is difficult to pinpoint these differences using Fig. 7, due to

closeness of fit across unequal dosage. In a study conducted by Tangjuank, et al. (2009b), where CNS-AC was used to remove Cr from aqueous solution, the maximum removal occur at 60 min contact time. Also, Fig. 7 curve follows the trend reported in Luka et al. (2023), where orange peel removal of Fe and Cu was experimented. Metal uptake was also reported to increase to a flatten curve peak point in Siripatana et al. (2017) during Pb detoxification; in Coelho et al. (2014) and Coelho et al. (2018) during Cd, Cr & Pb biosorption, and; in N'goran et al. (2018) during Pb & Cd removal from natural freshwater, all using CNS.

3.5 Final Concentration After AAS Analysis

Earlier in Fig. 3, EDX reveals C_i = 0 ppm of Cu in the water sample but a value of 0.17 mg L^{-1} for Fe. This void, prompt further analysis of the sample using the AAS analyzer, which reveals 0.63 mg L^{-1} for Cu and 0.17 mg L^{-1} for Fe, as obvious in Table 3. After adsorption at 10, 20, 40 and 60 min, the C_e of Cu and Fe were determined using AAS at each adsorbent dosage, which opens the door for calculating their respective REs.

Evidence of adsorption taking place is the reduction of the $C_i - C_e$ with time, as shown in Table 3 and Fig. 8. For Cu sorption, highest RE = 87.38% is recorded at 10 min and 0.40 CNS dosage, while at the same time and dose, RE = 99.47% for Fe sorption. That is, for effective sorption of the two heavy metals from the lake water sample, the contact time and CNS dose must be low. At any particular dosage, C_e of the heavy metal as well as the REs decreases with increase in contact time. For both Cu and Fe, the dosage could be ranked starting from one with the highest % removal in this order: 0.40 > 0.80 > 1.20 > 1.60 g. Table 3 also confirmed that the sorption of Fe (i.e., RE = 99.47, 97.12, 94.76 and 92.41%) at the lowest contact time (i.e., 10 min) is higher across all doses used than that of Cu (i.e., RE = 87.38, 86.90, 86.43 and 85.95%), over the entire CNS dosage utilized. It is hence deduced that Fe is best adsorbed, based on calculated q_e and RE values used as the decision variables. Since Cu is more present in the lake than Fe (0.63 > 0.17 mg L^{-1} C_i), it is still illogical to rate Fe sorption by CNS above Cu, even at equal specified dosage and contact times. A better selection criterion should be sought out from their estimated isotherm parameters from many existing models in the literature. This lack of clear distinguishing feature between Cu and Fe sorption using CNS biosorbent is illustrated as shown in similar trend depicted in Fig. 8.

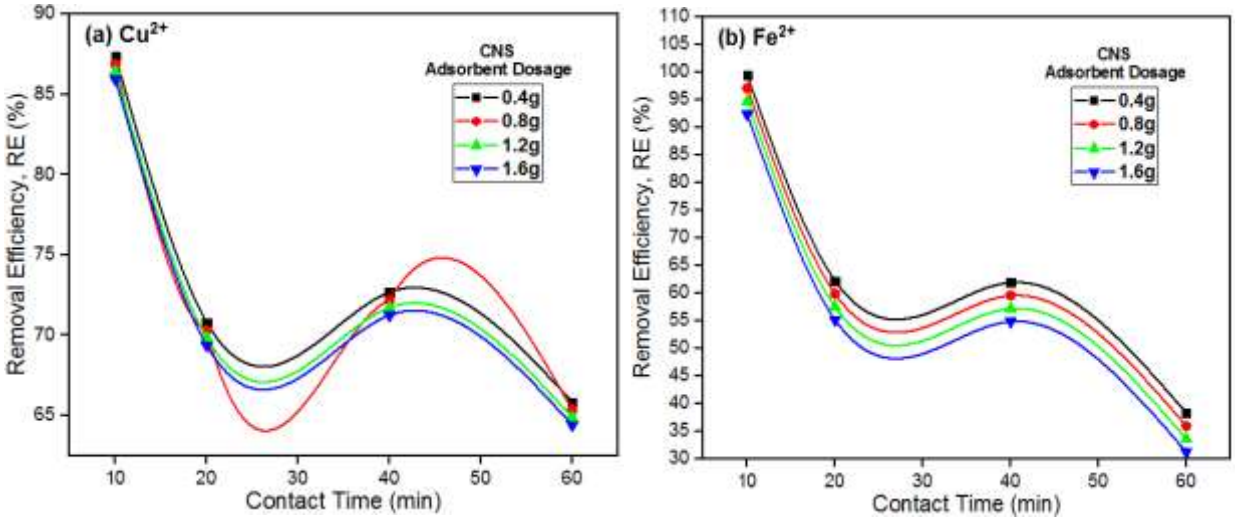

Fig. 8 Effect of Contact Time on Removal Efficiency of (a) Cu^{2+} and (b) Fe^{2+}.

Fig. 8 follows a smooth curved pattern with no complete overlapping of each representative adsorbent dosage line. One possible explanation for the erratic pattern is that the adsorption process may be influenced by the C_i of the metal ions in the solution. At higher C_i, the adsorbent may become saturated more quickly, leading to a decrease in % removal over time. A study carried out to investigate the performance CNS-AC in the removal of water hardness, gave an increasing RE with contact time [26], plus Christopher & Muthukumaran (2014) who arrived at the same curve trend when using equal blends of CNS and coconut shell AC to remove Cd.

Table 3 RE at four different adsorbent dosage.

	Cu			Fe		
CNS Dosage	C_i (mg L^{-1})	C_e (mg L^{-1})	**% Removal**	C_i (mg L^{-1})	C_e (mg L^{-1})	**% Removal**
0.40 g						
	0.63	0.0795	87.380952	0.17	0.0009	99.470588
	0.63	0.184	70.793651	0.17	0.0642	62.235294
	0.63	0.1721	72.68254	0.17	0.0647	61.941176
	0.63	0.2152	65.84127	0.17	0.1049	38.294118
0.80 g						
	0.63	0.0825	86.9047619	0.17	0.0049	97.1176471
	0.63	0.187	70.3174603	0.17	0.0682	59.8823529
	0.63	0.1751	72.2063492	0.17	0.0687	59.5882353
	0.63	0.2182	65.3650794	0.17	0.1089	35.9411765
1.20 g						
	0.63	0.0855	86.4285714	0.17	0.0089	94.7647059
	0.63	0.19	69.8412698	0.17	0.0722	57.5294118
	0.63	0.1781	71.7301587	0.17	0.0727	57.2352941
	0.63	0.2212	64.8888889	0.17	0.1129	33.5882353
1.60 g						
	0.63	0.0885	85.952381	0.17	0.0129	92.4117647
	0.63	0.193	69.3650794	0.17	0.0762	55.1764706
	0.63	0.1811	71.2539683	0.17	0.0767	54.8823529
	0.63	0.2242	64.4126984	0.17	0.1169	31.2352941

3.6 Route to the Selected Isotherm Model Parameters Determination

Axis values for a graphical determination of the 4 adsorption isotherm parameters is shown in Table 4 for each metallic ion. Since approximately equal q_e was given by each adsorbent value, Table 4 emanates from using C_e from the lowest adsorbent dosage of 0.40 g. Signs of $\log C_e$ and $\ln\left(\frac{C_e}{q_e}\right)$ in Table 4 is not a determining factor for the fitting of the Freundlich and Harkin-Jura model plots. The critical aspect is the relationship between these variables and the model parameters as per the linearized forms of the respective isotherm models.

Table 4 Axis variables values for relevant linearized isotherm plots.

C_e (mg L^{-1})	q_e (mg L^{-1})	$\frac{C_e}{q_e}$ (g L^{-1})	$\log C_e$	$\log q_e$	$\ln C_e$	$\ln\left(\frac{C_e}{q_e}\right)$	$\frac{1}{q_e^2}$ (mg g^{-1})$^{-2}$
Cu^{2+}							
0.0795	1.07	0.074299	-1.09963	0.029384	-2.532	-2.59966	0.873439
0.184	1.08	0.17037	-0.73518	0.033424	-1.69282	-1.76978	0.857339
0.1721	1.09	0.15789	-0.76422	0.037426	-1.75968	-1.84586	0.84168
0.2152	1.10	0.195636	-0.66716	0.041393	-1.53619	-1.6315	0.826446
Fe^{2+}							
0.0009	1.09	0.000826	-3.04576	0.037426	-7.01312	-7.09929	0.84168
0.0642	1.09	0.058899	-1.19246	0.037426	-2.74575	-2.83193	0.84168
0.0647	1.10	0.058818	-1.1891	0.041393	-2.73799	-2.8333	0.826446
0.1049	1.10	0.095364	-0.97922	0.041393	-2.25475	-2.35006	0.826446

Using Table 4 values, a plot of $\frac{C_e}{q_e}$ against C_e **(**Fig**.** 9**)** resulted in the Langmuir isotherm, where the slope is $\frac{1}{q_{max}}$ and the intercept is $\frac{1}{q_{max}\, k_L}$**.** In the same table, a plot of $\log q_e$ against $\log C_e$ values **(**Fig**.** 10**)**, resulted in the Freundlich isotherm line, whose slope and intercepts are $\frac{1}{n}$ and $\log K_f$, respectively**.** Fig**.** 11 is as a result of plotting $\ln\left(\frac{C_e}{q_e}\right)$ versus $\ln C_e$ with slope as β and intercept = $\ln A_{RP}$, which is the Redlich**-**Peterson representation**.** Harkin**-**Jura isotherm in Fig**.** 12 is normally obtained by plotting $\frac{1}{{q_e}^2}$ on y-axis and $\log C_e$ on the positive x-axis, where the intercepts is $\frac{B}{A}$ and slope is $\frac{1}{A}$**.** The straight**-**line equations in the graphs are alternative representations of the linearized models, which will aid the estimation of the unknown parameters in the isotherm models**.** Nevertheless, extent of fit of the dashed linear line to the few empirical data points in each plot is determined using the coefficient of determination **(**R^2**).**

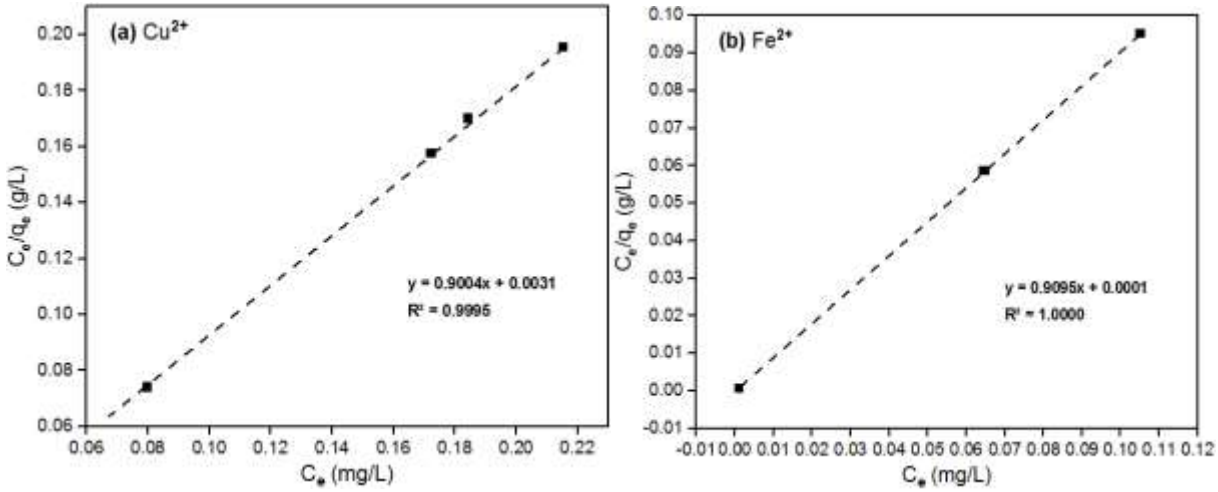

Fig. 9 Langmuir isotherm based on **(**a**)** copper and **(**b**)** iron data**.**

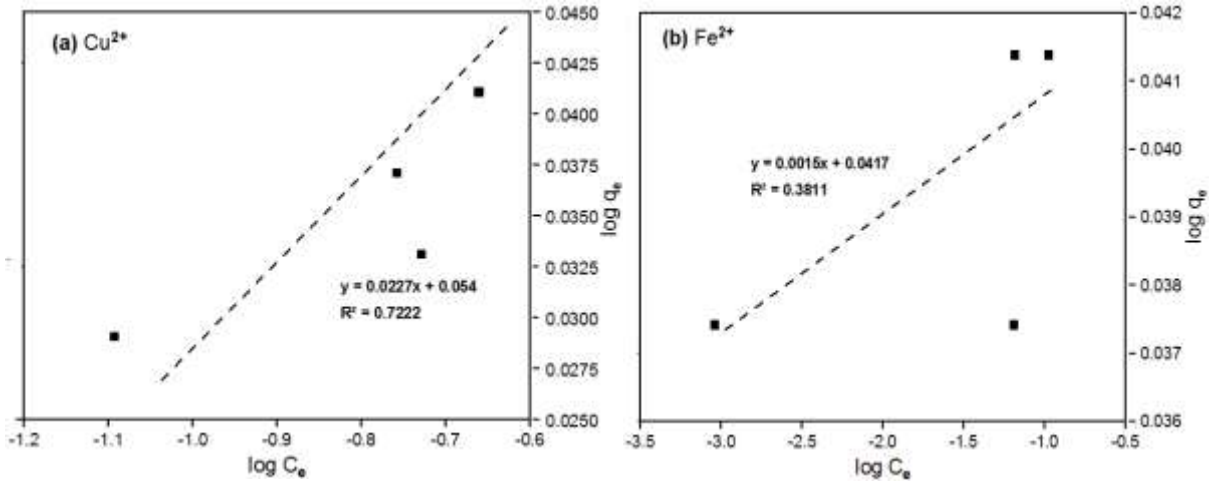

Fig. 10 Freundlich isotherm based on **(**a**)** Copper and **(**b**)** Iron data**.**

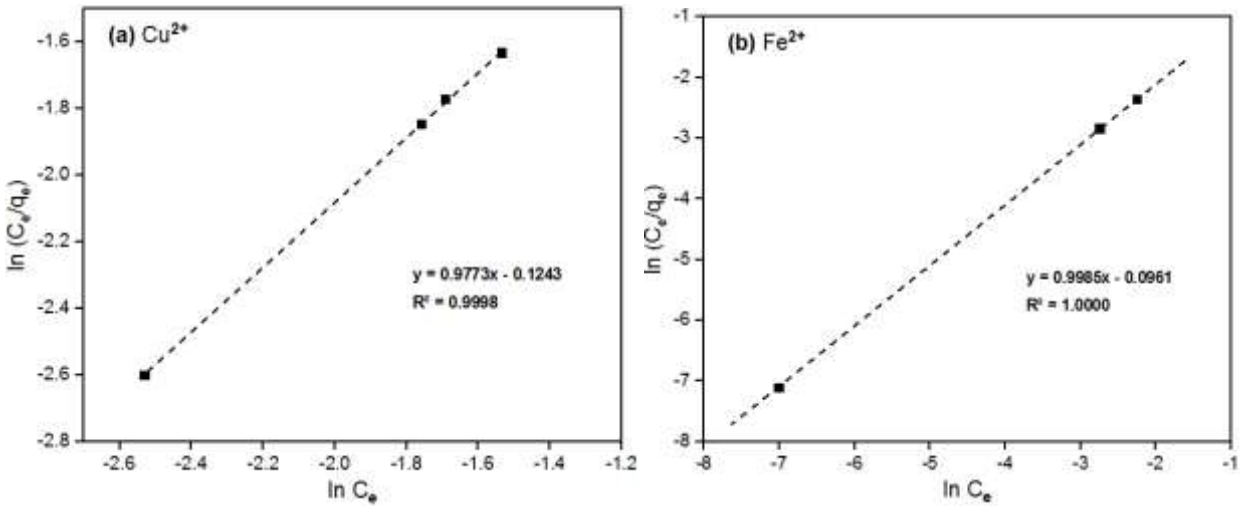

Fig. 11 Redlich-Peterson isotherm based on (a) Copper and (b) Iron data.

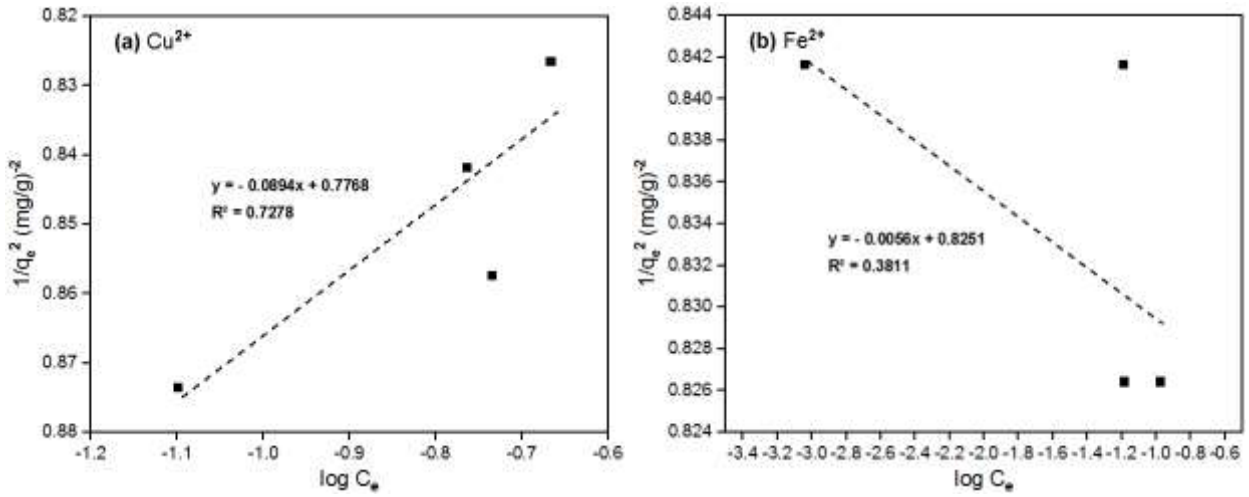

Fig. 12 Harkin-Jura isotherm based on (a) Copper and (b) Iron data.

Obviously, the Langmuir and the Redlich-Peterson isotherm models best describe the sorption data of Fe and Cu using CNS from the water sample. This is evidenced in their R^2 values of 0.9995 for Cu^{2+} and 1 for Fe^{2+} in Langmuir fitting and 0.9773 for Cu^{2+} and 1 for Fe^{2+} in Redlich-Peterson correlation. But because Fe R^2 is > Cu R^2 in just the 2 isotherms, Fe can be said to be the best heavy metal removed by the adsorbent. Seemingly, in Fig. 10 and 12, Freundlich and Harkin-Jura assumptions doesn't work with the sorption of Fe and Cu using CNS bio-adsorbent, due to lower R^2 values obtained. However, the fact that the description Cu^{2+} sorption of the poorly performed models leading to an R^2 = 0.7222 and 0.7278, respectively closer to 1, still raises hope as to whether further improvement of the process conditions will make it suitable. Sometimes, nonlinear regression graph fitting technique may give a good parameter estimate.

3.7 Model Performance

Table 5 showcased the adsorption parameters calculated from slopes and intercepts of Fig. (9) – (12). The q_{max} values for Cu and Fe are 1.1106 mg g^{-1} and 1.0995 mg g^{-1}, respectively, which indicates the maximum amount of metal ions that can be adsorbed per unit mass of the adsorbent at the given conditions. The higher the q_{max} value, the greater the adsorption capacity of the adsorbent for the metal ions. Previous analysis in Nuithitikul et al. (2020), resulted in q_{max} = 8.734 mg g^{-1} during Pb sorption by CNS, way above 1.1106 and 1.0995 mg g^{-1} predicted values from Langmuir equation/plot in this study. Moreso, the k_L value is related to the energy of adsorption and provides information about the affinity of the adsorbate (Fe & Cu) for the adsorbent (CNS). High k_L values (in both) indicate stronger affinity between the metal ion and CNS, suggesting a

more favorable adsorption process. It is stated in Augustine et al. (2019), that the value of $R_L < 1$ indicates favorable adsorption, while $R_L > 1$ suggests unfavorable adsorption. In this case, the R_L values for Cu and Fe are 5.4355 × 10^{-4} and **6.463** × 10^{-4}, respectively, indicating highly favorable adsorption for both metal ions.

A K_f = 1.39, 1.32, 1.741 and 1.197, 1.226 and 1.365, close to one obtained in this study (for Cu & Fe), was reported for Pb sorption using CNSL by Mdoe & Makene (2014), Cr sorption using CNS by Tangjuank, et al. (2009b), Cd sorption using CNS by Kumar et al. (2012a), and Cr, Pb & Cd sorption using CNS by Coelho et al. (2014), respectively. Hence, CNSL, a by-product of the cashew tree, is also a great adsorbent and Al corrosion controller, as ascertained by Fayomi et al. (2021) and as confirmed during the removal of Cr from aqueous solution by Wilson et al. (2014). Essentially, K_f value in the Freundlich model represents the adsorption capacity of the adsorbent and is an indicator of the adsorption strength. In this case, the adsorption of both Cu and Fe by the CNS adsorbent is characterized by a high adsorption capacity (as indicated by the K_f values). The exponent "n" in the Freundlich model is related to the surface heterogeneity and the favorability of adsorption. In **Table 5** Isotherm Parameters Obtained.

Model	**Parameter**	**Value**	
		Cu^{2+}	**Fe^{2+}**
Langmuir:	q_{max} (mg g^{-1})	1.1106	1.0995
	k_L (L mg^{-1})	290.456	9095.043
	R_L	5.4355 × 10^{-4}	6.463 × 10^{-4}
Freundlich:	K_f	1.1324	1.1008
	n	44.0529	666.6667
Redlich-Peterson:	β	0.9773	0.9985
	A_{RP}	1.1324	1.1009
Harkin-Jura:	A	11.1857	178.5714
	B	8.6891	147.3393

this case, the n values for Cu and Fe are 44.0529 and 666.6667, respectively [29, 33]. Higher "n" values in Table 5 indicates a more favorable adsorption process, suggesting a higher degree of non-linearity and heterogeneity in the adsorption process.

The parameter, β, represents the isotherm shape factor, which characterizes the deviation from linearity in the adsorption process. The values of β for Cu (0.9773) and Fe (0.9985) suggest a moderate deviation from linearity, indicating a relatively non-ideal adsorption behavior. But the parameter A_{RP} represents a combined constant in the Redlich-Peterson model. Values of A_{RP} for Cu (1.1324) and Fe (1.1009) provide information about the adsorption capacity and the effect of concentration on the adsorption process. Hence, it is equal to K_f. For Harkin-Jura, higher values of A and B for Fe compared to Cu suggest a stronger adsorption capacity and interaction for Fe compared to Cu using the CNS adsorbent, as evidenced in perfect fit of $R^2 = 1$.

4. Conclusion

CNS adsorbent for Fe and Cu data obtained by running a sorption experiment at 10 – 60 min equilibrium time, 0.40 – 1.60g biosorbent dosage, 8.05 pH and at pre-determined initial adsorbate concentration in water using AAS equipment, successfully facilitated the determination of isotherm parameters of Langmuir, Freundlich, Redlich-Peterson and Harkin-Jura models. These parameters contributed to a comprehensive understanding of the adsorption mechanisms and the effectiveness of the CNS adsorbent in removing Cu and Fe from aqueous Lake Gerio water solution. Before then, observed FTIR C-H functional group post-adsorption, change in surface morphology revealed by SEM afterwards and the observed reduction in heavy metal C_e, sufficiently makes CNS a good adsorbent. Moving forward, the R_L value estimated portrayed a favorable adsorption that perfectly fits only Langmuir and Redlich-Peterson isotherm models. Isotherm parameters like q_{max}, K_f and A_{RP} that describes the metals uptake are approximately equal. In Langmuir, predicted q_{max}, which is 1.1106 mg g^{-1} for Cu and 1.0995 mg/g for Fe are in close agreement with the actual empirical maximum of 1.10 mg g^{-1} for both Fe and Cu. Contributory to existing studies where Langmuir and Freundlich often fit better in majority of studies, this study discovered in addition, that Redlich-Peterson suits the sorption of Cu and Fe using CNS adsorbent. The entirety of metals removed in

previous studies and the kinetic or isotherm models used had been recorded in this study, with easily identifiable gaps that remains to be field by interesting researchers

Acknowledgements

Mr**.** Augustine Odey Egbeji extends his appreciations to his supervisors for a job well done in providing the needed guide in executing and completing his B**.**Eng**.** Degree research work at Modibbo Adama University, Nigeria in 2023**.**

References

[1] J. J. Christopher and K. Muthukumaran, Removal and recovery of Cd (II) from wastewater using chemically activated carbon composite, Int. J. Appl. Environ. Sci. 9(6) (2014) 2939–2958,

[2] P. S. Kumar, S. Ramalingam, R. V Abhinaya, K. V Thiruvengadaravi, P. Baskaralingam, S. Sivanesan, Lead (II) adsorption onto sulphuric acid treated cashew nut shell, Sep. Sci. Technol. 46 (15) 2011) 37 – 41.

[3] J. Wilson, J. Y. N. Philip, J. E. G. Mdoe, Synthesis of poly (APP-co-EGDMA) particles using monomers derived from cashew nut shell liquid for the removal of Cr (III) from aqueous solutions, Open J. Org. Polym. Mater. (4) (2014) 29 – 36,

[4] P. S. Kumar, S. Ramalingam, R. V Abhinaya, S. D. Kirupha, T. Vidhyadevi, S. Sivanesan, Adsorption equilibrium, thermodynamics, kinetics, mechanism and process design of zinc (II) ions onto cashew nut shell, Can. J. Chem. Eng. (90) (2012) 973 – 982.

[5] P. S. Kumar, S. Ramalingam, V. Sathyaselvabala, S. D. Kirupha, A. Murugesan, S. Sivanesan, Removal of cadmium (II) from aqueous solution by agricultural waste cashew nut shell, Korean J. Chem. Eng. 29(6) (2012) 756 – 768.

[6] J. Wang, Study on the performance identification of OpenCV in cashew nut shell-based activated carbon," in ESAET 2021: Earth and Environmental Science IOP Conference Series, 769 (2021) (032030) 1–10,

[7] A. Geczo, D. A. Giannakoudakis, K. Triantafyllidis, M. R. Elshaer, E. Rodriguez-Aguado, S. Bashkova, Mechanistic insights into acetaminophen removal on cashew nut shell biomass-derived activated carbons, Environ. Sci. Pollut. Res. (28) (2021) 58969 – 58982.

[8] M. A. Hassan, Biosorption of toxic metals/metalloids by fungi: A solution to contaminated soil, Direct Res. J. Chem. Mater. Sci. 11(4) (2023) 27 – 33.

[9] S. Fayanto, S. D. Naba, S. R. Ahmanas, N. Nugraha, Hunaidah, Adsorption of heavy metals based on the bio-removal method, in The 8th National Physics Seminar 2019, (2019) 2169 (060003) 1 – 7.

[10] R. Balakrishnan and S. Needhidasan, Analysis of substrate effects in Coovam River treatment using low cost adsorbent, Int. J. Pure Appl. Math. 119(17) (2018) 2885 – 2901.

[11] O. I. Sekunowo and G. U. Uduh, Extraction and physicochemical characterization of cashew nut-shell liquid in metal forming, Niger. J. Technol. Dev. 19(2) (2022) 110 – 115.

[12] A. B. Ngulde, K. Silas, H. D. Mohammed, A. L. Yaumi, U. H. Taura, H. H. Mari, Conversion of biomass to adsorbent: A review, Arid Zo. J. Eng. Technol. Environ. 18(1) (2022) 65 – 78.

[13] M. B. Ogundiran, J. O. Babayemi, C. G. Nzeribe, Determination of metal content and an assessment of the potential use of waste cashew nut ash (CNSA) as a source for potash production, BioResources 6(1) (2011) 529 – 536.

[14] S. Suresh, G. Vijayalakshmi, B. Rajmohan, V. Subbaramaiah, Adsorption of benzene vapor onto activated biomass from cashew nut shell: Batch and column study, Recent Patents Chem. Eng. (5) (2012) 116 – 133.

[15] S. H. Sanger, A. G. Mohod, Y. P. Khandetode, H. Y. Shrirame, A. S. Deshmukh, Study of carbonization for cashew nut shell, Res. J. Chem. Sci. 1(2) (2011) 43 – 55.

[16] P. P. Padhi and S. Dash, Determination of proximal attributes and physico-chemical properties of cashew nut (Annarcardium occidentale L.) oil and cashew nut shell liquid, Int. Adv. Res. J. Sci. Eng. Technol. 9(5) (2022) 209 – 214.

[17] T. F. Akinhanmi, V. N. Atasie, P. O. Akintokun, Chemical composition and physicochemical properties of cashew nut (Anacardium occidentale) oil and cashew nut shell liquid, J. Agric. Food, Environ. Sci. 2(1) (2008) 1 – 10.

[18] A. J. Tsamba, Fundamental study of two selected tropical biomass for energy: Coconut and cashew nut shells, Doctoral Thesis in Doctoral Thesis in Energy and Furnace Technology Stockholm, Sweden, 2008.

[19] S. H. Sengar, A. G. Mohod, Y. P. Khandetod, Performance evaluation of kiln for cashew nut shell carbonization and liquid, Int. J. Energy Eng. 2(3) (2022) 78 – 85.

[20] G. F. Coelho et al., Removal of Cd(II), Pb(II) and Cr(III) from water using modified residues of Anacardium occidentale L, Appl. Water Sci. 8(96) (2018) 1 – 21.

[21] N. Amaliyah and A. E. E. Putra, Microwave-assisted pyrolysis of cashew nut shell, Int. J. Des. Nat. Ecodynamics. 16(2) (2021) 227–232.

[22] D. Prabu, R. Parthiban, P. S. Kumar, N. Kumari, P. Saikia, Adsorption of copper ions onto nano-scale zero-valent iron impregnated cashew nut shell, Desalin. Water Treat. (57) (2016) 6487 – 6502.

[23] M. I. Papadaki, D. I. Mendoza-Castillo, H. E. Reynel-Avila, A. Bonilla-Petriciolet, S. Georgopoulos, Nut shells as adsorbents of pollutants: Research and perspectives, in Frontiers in Chemical Engineering 3 (640983, B. R. Bakshi, R. Mukherjee, J. G. S. Hernandez, Eds, 2021, pp. 1 – 15.

[24] T. J. Riwa, S. J. Mushi, M. M. Madirisha, P. E. Mabeyo, E. C. Mapunda, Exploring the circular prospects of cashew nutshells and avocado seeds as potential adsorbents for onboard natural gas storage. SSRN), 2023, pp. 1 – 17.

[25] E. C. Mwakobe, A column design for groundwater hardness removal using cashew nut shells activated carbon with potential application in low-income communities, Masters Theses and Dissertations [MEWES] Degree of Master's in Hydrology and Water Resources Engineering of the Nelson Mandela AFrican Institution of Science and Technology [NM-AIST] Repository, 2020.

[26] C. R. China, Adsorption studies on water hardness removal by using cashewnut shell activated carbon as an adsorbent, African J. Sci. Res. 5(4) (2016) 78 – 81.

[27] S. Tangjuank, N. Insuk, J. Tontrakoon, V. Udeye, Adsorption of lead (II) and cadmium (II) ions from aqueous solutions by adsorption on activated carbon prepared from cashew nut shells, World Acad. Sci. Eng. Technol. Int. J. Chem. Mol. Eng. 3(4) (2009) 221–227.

[28] K. F. S. de Oliveira et al., Cashew nut shell (Anarcadium accidentale L) charcoal as bioadsorbent to remove Cu2+ and Cr3+, Res. Soc. Dev. 10(2) (2021) 1 – 18.

[29] A. R. Haneef and S. S. Nair, Iron removal from water by using cashew nut shell, Int. J. Sci. Res. 6 (5) (2017) 2237 – 2242.

[30] V. A. Smith et al., The role of surface chemistry and polyethylenimine grafting in the removal of Cr (VI) by activated carbons from cashew nut shells, J. Carbon Res. 7(27) (2021) 1–15.

[31] S. Tangjuank, N. Insuk, V. Udeye, J. Tontrakoon, Chromium (III) sorption from aqueous solutions using activated carbon prepared from cashew nut shells, Int. J. Phys. Sci. 4(8) (2009) 412 – 417.

[32] P. S. Kumar, S. Ramalingam, S. D. Kirupha, A. Murugesan, T. Vidhyadevi, S. Sivanesan, Adsorption behavior of nickel(II) onto cashew nut shell: Equilibrium, thermodynamics, kinetics, mechanism and process design, Chem. Eng. J. 167(1) (2011) 122 – 131.

[33] K. Nuithitikul, R. Phromrak, W. Saengngoen, Utilization of chemically treated cashew-nut shell as potential adsorbent for removal of Pb (II) ions from aqueous solution, Sci. Rep. 10(3343) (2020)1–14.

[34] I. K. Tetteh, C. K. Gidisu, A. Sulemana, K. Miezah, Detoxification of E-waste polluted site using cashew nut shell-based activated carbon, Res. Sq. (2021) 1 – 44..

[35] P. S. Kumar, S. Ramalingam, V. Sathyaselvabala, S. D. Kirupha, S. Sivanesan, Removal of copper (II) ions from aqueous solution by adsorption using cashew nut shell, Desalination 266(1–3) (2011) 63 – 71.

[36] G. F. Coelho, A. C. Gonçalves, C. R. Tarley, J. Casarin, H. Nacke, M. A. Francziskowski, Removal of metal ions Cd (II), Pb (II), Cr (III) from water by the cashew nut shell Anacardium occidentale L, Ecol. Eng. (73) (2014) 514 – 525.

[37] K. P. D. A. N'goran et al., Lead and cadmium removal from natural freshwater using mixed activated carbons from cashew and shea nut shells, Arab. J. Geosci. 11(498) (2018) 1–13.

[38] P. S. Kumar, Adsorption of lead (II) Ions from simulated wastewater using natural waste: A kinetic, thermodynamic and equilibrium study, Environ. Prog. Sustain. Energy. 33(1) (2014) 55 – 64.

[39] L. M. Uwa, Heavy metal and microbial analysis of municipal water treatment plant, Int. J. Biosci. Technol. 9(9) (2016) 52 – 57.

[40] T. B. Wokhe, Heavy metals pollution of water and sediment in Mada River, Nigeria, J. Sci. Res. Reports 6(2) (2015) 157 – 164,.

[41] Y. M. Usman, A. Mohammed, B. Ibrahim, B. A. Saleh, Assessment of groundwater quality status along River Ngadda in Maiduguri, Nigeria, Int. J. Eng. Sci. 5(1) (2016) 8 – 14.

[42] R. T. Idowu, N. M. Inyang, H. M. G. Ezenwaji, Heavy metal concentrations in a West African Sahel reservoir, Anim. Res. Int. 1(1) (2004) 12 – 15.

[43] M. M. Aji, B. Gutti, B. K. Highina, Application of activated carbon in removal of iron and manganese from Alau Dam water in Maiduguri, Columbian J. Life Sci. 17(1) (2015) 35 – 39.

[44] Y. Luka, A. M. Abubakar, P. A. Adegoke, E. J. Kwaji, Optimization of sorption of lead and copper from Lake Gerio water sample by Aspergillus niger, J. Mater. Environ. Sci. 15(1) (2024) 1 – 24.

[45] R. Wuana, C. Ogbodo, A. U. Itodo, I. S. Eneji, Ecological and human health risk assessment of toxic metals in water, sediment and fish from Lower Usuma Dam, Abuja, Nigeria, J. Geosci. Environ. Prot. (8) (2020) 82 – 106.

[46] E. S. Danbauchi, Evaluation of lower Usuma Dam water quality for domestic supply (FCT) Abuja, Nigeria, Int. J. Res. Sci. Innov. VII (IX) (2020) 219 – 224.

[47] A. A. Bichi and S. L. Halliru, Determination of heavy metals along River Jakara in Urban Kano and their health implication; for sustainable development in Nigeria, in 2nd International Conference on Chemical, Biological and Environmental Engineering, Cairo, Egypt, 2010, pp. 220 – 224

[48] N. Abdullahi, E. C. Igwe, M. A. Dandago, Heavy metals contamination sources in Kano (Nigeria) and their concentrations along Jakara River and its agricultural produce, Moroccan J. Agric. Sci. 2(2) (2017) 106 – 113.

[49] M. B. Idris, K. D. Khalid, Z. Abdullahi, Comparative assessment of heavy metals concentration in the soil in the vicinity of tannery industries, Kumbotso Old Dump Site and River Challawa confluence, at Challawa Industrial Estate, Kano state, Nigeria, Int. J. Innov. Res. Dev. 4 (6) 122–128, 2015, [Online]. Available: www.ijird.com.

[50] S. Ibrahim and H. A. Sa'id, Heavy metals load in tilapia species: A case study of Jakara River and Kusalla Dam, Kano state, Nigeria, Bayero J. Pure Appl. Sci. 3(1) (2010) 87 – 90.

[51] Y. Luka, D. O. Patrick, H. M. Kefas, Q. Amawo, Biosorption of copper and iron ions from Shinko drainage wastewater in Jimeta-Yola using orange peels, Savannah J. Sci. Eng. Technol. 1(6) (2023) 352 – 359.

[52] K. B. Guillaume, N. S. Serpokrylov, A. S. Smolyanichenko, E. G. Cheblakova, V. A. Gorina, Preparation of activated carbon from cashew nut shells for water purification, Процессы получения и свойства порошков. (2) (2019) 15 – 22.

[53] Hunaidah, M. A. A. Undu, S. Fayanto, Sulwan, K. Y. Setiawan, Activated carbon from cashew nut waste and its application as a heavy metal absorbent, in 5th ICMSE 2018 Conference Series in Journal of Physics, 1321(022004) (2019) 1 – 6.

[54] M. D. Yahya, A. S. Aliyu, K. S. Obayomi, A. G. Olugbenga, U. B. Abdullahi, Column adsorption study for the removal of chromium and manganese ions from electroplating wastewater using cashew nutshell adsorbent, Cogent Eng. 7(1) (2020) 1 – 18.

[55] B. K. Vidyashree, D. P. Nagarajappa, N. T. Manjunath, K. Manjunatha, Investigative study on the treatment of domestic wastewater by soil aquifer treatment (SAT) in conjunction with cashew nut shell adsorbent, Int. J. Sci. Adv. Res. Technol. 2(11) (2016) 192–195.

[56] A. U. Augustine, B. Ishaq, T. M. Akpomie, R. Odoh, Removal of lead (II) and iron (II) ions from aqueous solutions using watermelon (Citrillus lanatus) peels as adsorbent, Open Access J. Chem. 3(1) (2019) 1 – 7.

[57] N. Ayawei, A. N. Ebelegi, D. Wankasi, Modelling and interpretation of adsorption isotherms, J. Chem. 2017(3039817) (2017) 1 – 12.

[58] C. Siripatana, A. Khuenpetch, R. Phromrak, Kinetic study of adsorption of lead (II) ions onto cashew nut shells, ARPN J. Eng. Appl. Sci. 12(7) (2017) 1819 – 1824.

[59] J. E. G. Mdoe and J. S. Makene, Removal of lead(II) ions from aqueous solutions using cashew nut shell liquid-templated thiol-silica materials, Bull. Chem. Soc. Ethiop. 28(3) (2014) 363 – 372.

[60] O. M. Fayomi, D. C. Ike, M. A. Iorhemba, O. M. Ameh, N. E. Ihegwuagu, R. C. Kalu, Investigation on the corrosion inhibiting property of modified cashew nutshell liquid, Int. J. Corros. Scale Inhib. 10 (3) (2021) 1307 – 1322.